

Differences in chemical doping matter - Superconductivity in $\text{Ti}_{1-x}\text{Ta}_x\text{Se}_2$ but not in $\text{Ti}_{1-x}\text{Nb}_x\text{Se}_2$

Huixia Luo^{1,*}, Weiwei Xie¹, Jing Tao², Ivo Pletikoscic^{2,3}, Tonica Valla², Girija S. Sahasrabudhe¹, Gavin Osterhoudt⁴, Erin Sutton⁴, Kenneth S. Burch⁴, Elizabeth M. Seibel¹, Jason W. Krizan¹, Yimei Zhu² and Robert J. Cava¹

¹*Department of Chemistry, Princeton University, Princeton, NJ 08544, USA*

²*Condensed Matter Physics and Materials Science Department, Brookhaven National Lab, Upton, New York 11973, USA*

³*Department of Physics, Princeton University, Princeton, NJ 08544, USA*

⁴*Department of Physics, Boston College, 140 Commonwealth Ave Chestnut Hill, Boston, MA 02467-3804, USA*

ABSTRACT

We report that 1T-TiSe₂, an archetypical layered transition metal dichalcogenide, becomes superconducting when Ta is substituted for Ti but not when Nb is substituted for Ti. This is unexpected because Nb and Ta should be chemically equivalent electron donors. Superconductivity emerges near $x = 0.02$ for $\text{Ti}_{1-x}\text{Ta}_x\text{Se}_2$, while for $\text{Ti}_{1-x}\text{Nb}_x\text{Se}_2$, no superconducting transitions are observed above 0.4 K. The equivalent chemical nature of the dopants is confirmed by X-ray photoelectron spectroscopy. ARPES and Raman scattering studies show similarities and differences between the two systems, but the fundamental reasons why the Nb and Ta dopants yield such different behavior are unknown. We present a comparison of the electronic phase diagrams of many electron-doped 1T-TiSe₂ systems, showing that they behave quite differently, which may have broad implications in the search for new superconductors. We propose that superconducting $\text{Ti}_{0.8}\text{Ta}_{0.2}\text{Se}_2$ will be suitable for devices and other studies based on exfoliated crystal flakes.

KEYWORDS: Superconductivity; Dichalcogenide; $\text{Ti}_{1-x}\text{Ta}_x\text{Se}_2$; $\text{Ti}_{1-x}\text{Nb}_x\text{Se}_2$

*huixial@princeton.edu

INTRODUCTION

Layered transition-metal dichalcogenides (TMDs) have been studied for decades as archetypical examples of materials where superconductivity is balanced against a competing charge density wave (CDW) state.¹⁻¹⁰ The superconducting and CDW transition temperatures in this family can be tuned by changing electron count through chemical substitution or intercalation (e.g. refs. 11-13), using high pressure (e.g. refs. 14-17), or gating¹⁸). 1T-TiSe₂ is one of the simplest and most widely studied TMDs, undergoing a transition to a CDW state at about 200 K in its native form¹⁹ and becoming a superconductor when put under pressure or electron doped through intercalation. In Cu_xTiSe₂, Cu donates electrons to the TiSe₂ layers, and superconductivity is induced with a maximum T_c of 4.2 K. This observation has triggered a great deal of recent activity on long-studied 1T-TiSe₂ (e.g. refs 13, and 19-24), especially as the superconducting phase is proposed to be an example of an exciton condensate. Similarly, Pd-intercalated TiSe₂ is also superconducting.²⁴

Here we report the observation of superconductivity in 1T-TiSe₂ induced by doping with electrons through partial substitution of Ta for Ti, in materials of the type Ti_{1-x}Ta_xSe₂. We find that for Ti_{1-x}Ta_xSe₂ the CDW transition remains present and a superconducting state emerges near $x = 0.02$ with a maximum T_c of 2.2 K at $x = 0.2$. In contrast, we find that similarly made and tested isostructural and chemically isoelectronic Ti_{1-x}Nb_xSe₂ is not superconducting above 0.4 K. This is unexpected because both Nb and Ta have 5 valence electrons, and thus should simply donate their electrons to the conduction band of 1T-TiSe₂, which is dominated by normally empty Ti (4 valence electrons) electronic states. This conventional electronic picture is verified by our chemical spectroscopy (X-ray photoelectron spectroscopy (XPS)) measurements, and our ARPES characterization of the materials shows that electrons are indeed donated to the formerly empty conduction band in 1T-TiSe₂ by both substitutions, but also that there are some significant differences. Consistent with the ARPES characterization, the Nb substitution leads to a lower electronic density of states than the Ta substitution, inferred from specific heat measurements. Further the Nb substituted material shows non-metallic resistivity behavior, in contrast to the metallic and superconducting behavior induced by Ta substitution. Finally, we construct a composition-dependent superconductivity phase diagram for many dopants in the archetype 1T-TiSe₂ system, comparing Ti_{1-x}Ta_xSe₂, Ti_{1-x}Nb_xSe₂, Pd_xTiSe₂ and Cu_xTiSe₂. The phase diagram shows that the superconductivity that is

induced in doped 1T-TiSe₂ is dramatically dependent on the chemical method used to change its electron count. This result for the TMD 1T-TiSe₂ is in contrast to what is found for other important superconducting systems, such as the iron arsenides, where substitutions of many different kinds induce nearly equivalent maximum superconducting T_c's at the same electron count.²⁵⁻²⁷ Our results show that what appear to be chemically equivalent electron donors are in fact not at all electronically equivalent in this system. If this is frequently the case, then it raises significant general issues in the search for superconductivity in all doped materials, where chemically equivalent dopants are only rarely individually tested.

EXPERIMENTAL SECTION

Polycrystalline samples of Ti_{1-x}Ta_xSe₂ and Ti_{1-x}Nb_xSe₂ were synthesized in two steps by solid state reaction. First, the mixtures of high-purity fine powders of Ta (99.8%) or Nb (99.8%), Ti (99.9%) and Se (99.999%) in the appropriate stoichiometric ratios were thoroughly ground, pelletized and heated in sealed evacuated silica tubes at a rate of 1 °C/min to 700 °C and held there for 120 h. Subsequently, the as-prepared powders were reground, re-pelletized, and sintered again, heated at a rate of 3 °C/min to 700 °C and held there for 120 h. Single crystals of selected compositions were grown by the chemical vapor transport (CVT) method with iodine as a transport agent. Two-gram as-prepared powders of Ti_{0.8}Ta_{0.2}Se₂ or Ti_{0.8}Nb_{0.2}Se₂ were mixed with 100 mg iodine, sealed in evacuated silica tubes and heated for one week in a two zone furnace, where the temperature of source and growth zones were fixed at 675 °C and 725 °C, respectively. The identity and phase purity of the samples were determined by powder X-ray diffraction (PXRD) using a Bruker D8 Advance ECO with Cu K α radiation and a LYNXEYE-XE detector. To determine the unit cell parameters, LeBail fits were performed on the powder diffraction data through the use of the FULLPROF diffraction suite using Thompson-Cox-Hastings pseudo-Voigt peak shapes.²⁸ Single crystals selected from partially crushed crystalline samples were employed for the single crystal structure determinations.

Measurements of the temperature dependence of the electrical resistivity (4 contact), specific heat and magnetic susceptibility of the materials were performed in a Quantum Design Physical Property Measurement System (PPMS). There was no indication of air-sensitivity of the materials during sample preparation. Selected

resistivities and heat capacities were measured in the PPMS equipped with a ^3He cryostat. Magnetic susceptibility characterization for $\text{Ti}_{0.8}\text{Ta}_{0.2}\text{Se}_2$ and $\text{Ti}_{0.8}\text{Nb}_{0.2}\text{Se}_2$ was carried out in a 5T applied AC field. Specimens for the electron diffraction studies in a transmission electron microscope were obtained from synthesized samples crushed in a dry box and transported to the microscope in ultra-high vacuum. Temperature-dependent electron diffraction measurements were performed at Brookhaven National Laboratory on a JEOL 2100F microscope equipped with a liquid-helium cooled sample holder. The angle-resolved photoelectron spectroscopy (ARPES) measurements were conducted at beamlines 10 and 12 of Advanced Light Source, Lawrence Berkeley National Laboratory using Scienta electron analyzers set to overall resolution of 25 meV and 0.3° . Two-dimensional angular maps were assembled at BL10 from multiple line scans taken by rotating the analyzer around the axis parallel to its slit. Samples were cleaved at 15 K in ultrahigh vacuum of 5×10^{-9} Pa and all the data were collected at 15 K. The phonon spectra of Nb- and Ta- doped TiSe_2 were probed using micro-Raman spectroscopy. In layered TMDs this can be challenging due to their strong tendency to oxidize at the surface. Thus we performed the experiments entirely in a glovebox with argon atmosphere, with samples being freshly cleaved just before the measurement. This was achieved with a WITec alpha300R spectrometer customized to work inside an Ar-filled glovebox. The sample was excited with unpolarized light at 532 nm with the reflected and Raman scattered light collected in a backscattering configuration. The reflected light was removed using an edge filter, resulting in a lower cut-off of 85 cm^{-1} . To avoid unwanted heating, the power was kept below 20 μW and focused to a spot size approximately 1 μm in diameter. Results shown are the average of at least 6 such measurements, corrected for the integration time and laser power. To confirm the single crystal nature and reproducibility, all spectra were confirmed by measuring spots millimeters apart.

X-ray Photoelectron Spectroscopy (XPS) characterization was performed with a VG ESCA Lab Mk.II instrument. All spectra were obtained using Mg $K\alpha$ radiation (1284 eV) and 20 eV pass energy. NbSe_2 , $\text{Ti}_{0.8}\text{Nb}_{0.2}\text{Se}_2$, $\text{Ti}_{0.8}\text{Ta}_{0.2}\text{Se}_2$ polycrystals and TaSe_2 single crystals were placed on carbon tape attached to separate metal sample holders. Usually, the Carbon 1s (C1s) peak originating from adventitious carbon on the sample surface is used for calibration purposes. But as the samples were polycrystalline, C1s signal from the carbon tape could not be obviated. Thus, to compensate for the charging effects, the sample holders were biased at +10 volts ²⁹.

Since, the surface of the polycrystals and single crystals were oxidized due to ambient oxidation; TiO_2 , Nb_2O_5 , Ta_2O_5 formed at the surface of the samples were used for comparison and calibration. All scans were taken with a 0.05 eV step size and 0.5 s dwell time. The resolution of the instrument is less than 0.1 eV. The obtained scans were fit with Casa XPS using a Shirley background, area and positions were constrained using standard values.

Results and Discussion

First we consider the chemistry and structures of the $\text{Ti}_{1-x}\text{Ta}_x\text{Se}_2$ and $\text{Ti}_{1-x}\text{Nb}_x\text{Se}_2$ systems. 1T- TiSe_2 is a layered compound with trigonal symmetry.³⁰ The Ti atoms, which are in octahedral coordination with Se, form planar TiSe_2 layers of edge sharing octahedra. These layers are bonded to each other by van der Waals forces. Previous work has shown that when Cu atoms are intercalated to form the Cu_xTiSe_2 superconductor, they occupy positions between the TiSe_2 layers.¹³ Here we find from our high quality single crystal structural analyses of $\text{Ti}_{0.9}\text{Ta}_{0.1}\text{Se}_2$ and $\text{Ti}_{0.8}\text{Nb}_{0.2}\text{Se}_2$ that when Ta or Nb atoms are substituted for Ti, they substitute directly on the Ti site, replacing some of the Ti in the octahedra. There are no interstitial atoms in either case, to a high level of precision, and both structures are that of ideal 1T- TiSe_2 (see **Table 1S** and **Table 2S** Supplementary Information). **Figure 1a** shows the powder x-ray diffraction patterns for selected members of both families. The results show that single phase solid solutions are indeed formed in these systems. The solubility limit for intercalated Cu in TiSe_2 is $x \approx 0.11$. However, in the substitution case, the solubility limits for $\text{Ti}_{1-x}\text{Ta}_x\text{Se}_2$ and $\text{Ti}_{1-x}\text{Nb}_x\text{Se}_2$ in the 1T structure phase are $x \approx 0.9$ and $x \approx 0.7$, respectively; at higher doping contents, the 2H-type TMDC structure is found for both $\text{Ti}_{1-x}\text{Ta}_x\text{Se}_2$ and $\text{Ti}_{1-x}\text{Nb}_x\text{Se}_2$.

The composition dependence of the room temperature lattice parameters for 1T- $\text{Ti}_{1-x}\text{Ta}_x\text{Se}_2$ ($0 \leq x \leq 0.9$), 1T- $\text{Ti}_{1-x}\text{Nb}_x\text{Se}_2$ ($0 \leq x \leq 0.7$), and a comparison to those for 1T- Cu_xTiSe_2 ($0 \leq x \leq 0.11$) are shown in **Figure 1b**. The a parameters increase through both substitution of Ta or Nb and intercalation of Cu in TiSe_2 , but the c parameters change in an opposite fashion for substitution vs. intercalation: c decreases with increasing Ta or Nb substitution in $\text{Ti}_{1-x}(\text{Ta/Nb})_x\text{Se}_2$, while it increases with increasing Cu intercalation in Cu_xTiSe_2 ($0 \leq x \leq 0.11$). The fact that the lattice parameters track each other so well in the two cases is an indirect indication that the

Nb and Ta doped systems are structurally analogous. The anomalous c axis behavior of Cu_xTiSe_2 has been previously noted.¹³

Superconductivity emerges near $x = 0.02$ for $\text{Ti}_{1-x}\text{Ta}_x\text{Se}_2$, while for $\text{Ti}_{1-x}\text{Nb}_x\text{Se}_2$, no superconducting transitions are observed above 0.4 K in the broad composition range of $0 \leq x \leq 0.7$. Looking to find differences in the chemistry of two systems, we performed XPS studies $\text{Ti}_{0.8}\text{Ta}_{0.2}\text{Se}_2$ and $\text{Ti}_{0.8}\text{Nb}_{0.2}\text{Se}_2$, as shown in **Figure 1 e, f**. For comparison, the Nb $3d$ and Ta $4f$ spectra for undoped 2H-NbSe₂ and 2H-TaSe₂ are included in **Figure 1 c, d**. The binding energy of the Ta $4f_{7/2}$ peak in TaSe₂ is 0.8 eV lower than that in $\text{Ti}_{0.8}\text{Ta}_{0.2}\text{Se}_2$. The binding energy of the Ta $4f_{7/2}$ peaks corresponding to Ta₂O₅ formed at the surface of TaSe₂ and $\text{Ti}_{0.8}\text{Ta}_{0.2}\text{Se}_2$ is 26.5 eV³¹ Similarly, the binding energy of the Nb $3d_{5/2}$ peak in NbSe₂ is 1.2 eV lower than that in $\text{Ti}_{0.8}\text{Nb}_{0.2}\text{Se}_2$. The binding energy of the Nb $3d_{5/2}$ peaks corresponding to Nb₂O₅ formed at the surface of NbSe₂ and $\text{Ti}_{0.8}\text{Nb}_{0.2}\text{Se}_2$ is 207.5 eV³² Thus, both Ta and Nb are more oxidized (i.e. have formal oxidation states between 4+ and 5+) when used as dopants in TiSe₂ than in the individual selenides. The relative shifts in binding energies are the same for both species, indicating that as chemical dopants they are indeed equivalent in 1T-TiSe₂. The Ti $2p$ and Se $3d$ XP spectra for both $\text{Ti}_{0.8}\text{Ta}_{0.2}\text{Se}_2$ and $\text{Ti}_{0.8}\text{Nb}_{0.2}\text{Se}_2$ are identical³³ as shown in **Figures 1S and 2S** (Supporting Information) further supporting the chemical equivalence of the two systems

We next consider the transport properties of the two systems. A systematic change in the temperature dependence of the resistivity of $\text{Ti}_{1-x}\text{Ta}_x\text{Se}_2$ occurs on increasing x . **Figure 2a** shows the temperature dependence of the normalized electrical resistivity ($\rho/\rho_{300\text{K}}$) for polycrystalline samples of $\text{Ti}_{1-x}\text{Ta}_x\text{Se}_2$ ($0 \leq x \leq 0.3$). At low temperatures, a clear, sharp ($\Delta T_c < 0.1$ K) drop of $\rho(T)$ is observed in the doped samples, signifying the onset of superconductivity at low temperatures in $\text{Ti}_{1-x}\text{Ta}_x\text{Se}_2$ for $x > 0.02$; as the $\text{Ti}_{1-x}\text{Ta}_x\text{Se}_2$ compounds become better metals, superconductivity emerges. The Ta substituted sample with $x = 0.2$ shows the highest T_c , 2.2 K (inset of **Figure 2a**). In addition, the signature of the CDW transition is seen for the low x content samples through the presence of the maxima in $\rho(T)$; at higher doping content the signature of the CDW transition gets much weaker.

The temperature dependence of the normalized electrical resistivities ($\rho/\rho_{300\text{K}}$) for the polycrystalline samples of $\text{Ti}_{1-x}\text{Nb}_x\text{Se}_2$ ($0 \leq x \leq 0.7$) are shown in **Figure 2b**. In contrast to the situation for $\text{Ti}_{1-x}\text{Ta}_x\text{Se}_2$, non-metallic behavior is clearly observed. We

examine the non-metallic behavior more closely in **Figure 2c**. The figure shows that the low temperature data can be fit by a two-dimensional variable range hopping model $\rho(T) = \rho_0 \exp(T_0/T)^n$, where T_0 is the characteristic Mott temperature, which depends on the electronic structure, the density of states near the Fermi level and localization length, ρ_0 is the pre-exponential factor and $n = 1/(d+1)$ for d -dimensional variable range hopping.³⁴ The materials are clearly not semiconducting at low temperatures, for which $n = 1$, although at higher temperatures the behavior appears to be semiconducting, with an activation energy of $E_A = 0.17$ eV. No superconducting transition is seen in any of the Nb substituted samples down to 0.4 K.

Hall measurement data confirms that both the $\text{Ti}_{1-x}\text{Ta}_x\text{Se}_2$ and $\text{Ti}_{1-x}\text{Nb}_x\text{Se}_2$ materials are n -type as expected for electron doping of 1T-TiSe₂; the larger negative Hall resistivity and its increase in magnitude with decreasing temperature for $\text{Ti}_{0.8}\text{Nb}_{0.2}\text{Se}_2$ (**Figure 2d inset**) is consistent with a lower n -type carrier concentration than in the Ta doping case. Further, **Figure 2d** shows that in neither case does the substitution in 1T-TiSe₂ lead to localized magnetic states; induced magnetism being a possible reason for the differences in behavior for the two systems. The susceptibilities are diamagnetic, dominated by the core diamagnetism, and the small Curie tails at low temperatures are from a very small fraction (sub percent) of spin-bearing defects. Thus magnetism induced by doping cannot be behind the difference in the electronic behavior observed in the two systems.

We next consider a comparison of the low temperature specific heats of the two systems and the thermodynamic characterization of the new superconductor. **Figure 2e** shows the specific heat data employed in order to further investigate the electronic properties and superconductivity in the optimal $\text{Ti}_{1-x}\text{Ta}_x\text{Se}_2$ superconductor. The main panel of **Figure 2e** shows the temperature dependence of the specific heat (C_p/T versus T^2) under zero-field and under 5 Tesla field for $\text{Ti}_{0.8}\text{Ta}_{0.2}\text{Se}_2$. For comparison, the temperature dependence of the zero-field specific heat (C_p/T versus T^2) for $\text{Ti}_{0.8}\text{Nb}_{0.2}\text{Se}_2$ is shown in **Figure 2f**. In both materials, the specific heat at low temperatures (but above T_c) obeys the relation of $C_p = \gamma T + \beta T^3$, where γ and β describe the electronic and phonon contributions to the heat capacity, respectively, the latter of which is a measure of the Debye Temperature (θ_D), and the former of which is the Sommerfeld parameter. By fitting the data in the temperature range of 2 - 10 K, we obtain the electronic specific heat coefficient $\gamma = 1.99$ mJ·mol⁻¹·K⁻², and the

phonon specific heat coefficient $\beta = 0.701 \text{ mJ}\cdot\text{mol}^{-1}\cdot\text{K}^{-4}$ for $\text{Ti}_{0.8}\text{Ta}_{0.2}\text{Se}_2$. Fitting the data for $\text{Ti}_{0.8}\text{Nb}_{0.2}\text{Se}_2$ similarly yields $\gamma = 0.45 \text{ mJ}\cdot\text{mol}^{-1}\cdot\text{K}^{-2}$ and $\beta = 0.475 \text{ mJ}\cdot\text{mol}^{-1}\cdot\text{K}^{-4}$. We can estimate the Debye temperatures by using the values of β , and $\theta_D = (12\pi^4 nR/5\beta)^{1/3}$, where n is the number of atoms per formula unit ($n = 3$), and R is the gas constant. The θ_D values are thus calculated to be 202 K for $\text{Ti}_{0.8}\text{Ta}_{0.2}\text{Se}_2$ and 230 K for $\text{Ti}_{0.8}\text{Nb}_{0.2}\text{Se}_2$. Finally, it can be seen that γ in $\text{Ti}_{0.8}\text{Ta}_{0.2}\text{Se}_2$ is nearly 5 times of that of $\text{Ti}_{0.8}\text{Nb}_{0.2}\text{Se}_2$. Since the value of γ is proportional to the electronic density of states (DOS) near the Fermi level (E_F), and the DOS near E_F has a very strong influence on T_c , this difference is likely a major factor in the lack of a superconducting transition in the Nb case. These data do not, however, tell us why the nominally equivalent Nb doping and Ta doping of 1T-TiSe₂ yield such different γ s.

$\text{Ti}_{0.8}\text{Ta}_{0.2}\text{Se}_2$ displays a large specific heat jump associated with a transition to superconductivity at T_c , as shown in the insets for **Figures 2e and f**. The superconducting transition temperature observed in the specific heat measurements for $\text{Ti}_{0.8}\text{Ta}_{0.2}\text{Se}_2$ is in excellent agreement with the T_c determined in the $\rho(T)$ measurements. From the inset in **Figure 2a**, using the equal area construction method, we obtain $\Delta C/T_c = 3.78 \text{ mJ mol}^{-1} \text{ K}^{-2}$ for $\text{Ti}_{0.8}\text{Ta}_{0.2}\text{Se}_2$. The normalized specific heat jump value $\Delta C/\gamma T_c$ is thus found to be 1.9 for $\text{Ti}_{0.8}\text{Ta}_{0.2}\text{Se}_2$, somewhat higher than that of the Bardeen-Cooper-Schrieffer (BCS) weak-coupling limit value (1.43), confirming bulk superconductivity. Using the Debye temperature (θ_D), the critical temperature T_c , and assuming that the electron-phonon coupling constant (λ_{ep}) can be

$$\lambda_{ep} = \frac{1.04 + \mu^* \ln\left(\frac{\theta_D}{1.45T_c}\right)}{(1 - 0.62\mu^*) \ln\left(\frac{\theta_D}{1.45T_c}\right) - 1.04},$$

calculated from the inverted McMillan formula³⁵: the value of λ_{ep} obtained is 0.61 for $\text{Ti}_{0.8}\text{Ta}_{0.2}\text{Se}_2$. This suggests weak coupling superconductivity. The density of states at the Fermi level ($N(E_F)$) can be calculated

from
$$N(E_F) = \frac{3}{\pi^2 k_B^2 (1 + \lambda_{ep})} \gamma$$
 by using the value of γ and the electron-phonon coupling (λ_{ep}). This yields $N(E_F) = 0.53 \text{ states/eV f.u.}$ for this system's optimal superconductor $\text{Ti}_{0.8}\text{Ta}_{0.2}\text{Se}_2$.

The superconducting transition for the optimal superconducting sample was further examined through temperature dependent measurements of the electrical resistivity under applied magnetic field. The $\rho(T,H)$ obtained for $\text{Ti}_{0.8}\text{Ta}_{0.2}\text{Se}_2$ is

presented in the supplementary information, **Figure 3S**. Based on the T_c determined for different magnetic fields, the upper critical field values, $\mu_0 H_{c2}$, are plotted vs. temperature in the inset to **Figures 3S**. A clear linear dependence of $\mu_0 H_{c2}$ vs. T is seen near T_c ; the solid line through the data shows the best linear fit with the initial slope $dH_{c2}/dT = -1.4$ T/K for both $Ta_{0.2}Ti_{0.8}Se_2$ and $Ta_{0.15}Ti_{0.85}Se_2$. We estimate the zero temperature upper critical field $\mu_0 H_{c2} = 2.23$ T for $Ti_{0.8}Ta_{0.2}Se_2$ (and 2.21 T for $Ta_{0.15}Ti_{0.85}Se_2$) using the Werthamer-Helfand-Hohenberg (WHH) expression, $\mu_0 H_{c2} = -0.693T_c (dH_{c2}/dT_c)^{36-38}$. The upper critical field $\mu_0 H_{c2}(0)$ calculated for $Ti_{0.8}Ta_{0.2}Se_2$ is larger than that reported for the $Cu_{0.08}TiSe_2$, ($T_c = 4.15$ K, $\mu_0 H_{c2}(0) = 1.33$ T).¹³

From $\mu_0 H_{c2} = \frac{\phi_0}{2\pi\xi_{GL}^2}$, where ϕ_0 is the quantum of flux, the Ginzburg-Landau coherence length can be estimated as $\xi_{GL}(0) \sim 120$ Å for $Ti_{0.8}Ta_{0.2}Se_2$.

Returning to the comparison of the two systems, we consider their characterization by low temperature electron diffraction, which is an excellent probe of the existence of CDWs in layered dichalcogenides.⁹ Thus in **Figures 1g-j** we compare the electron diffraction patterns in the [001] diffraction zones for both $Ti_{0.8}Ta_{0.2}Se_2$ and $Ti_{0.8}Nb_{0.2}Se_2$, determined in the TEM experiments at both ambient temperature and 89 K, the latter temperature chosen to be low enough to probe the possible presence of a CDW. Through these patterns we can determine whether the presence of superconductivity in the Ta one case but not in the Nb case has to do with whether the CDW is more efficiently suppressed through the doping, thus tipping the CDW-superconductivity balance toward the latter. The results are initially surprising. They show that the $(\frac{1}{2}, \frac{1}{2}, \frac{1}{2})$ superlattice due to the CDW is very weak or absent at 89 K in non-superconducting $Ti_{0.8}Nb_{0.2}Se_2$ but is clearly present in superconducting $Ti_{0.8}Ta_{0.2}Se_2$. Thus the appearance of superconductivity in the Ta-doped case cannot be due to a more efficient suppression of the CDW by Ta doping. The CDW in $TiSe_2$, however, is far from conventional in character and the literature remains divided on its origin.¹³⁻¹⁵ Therefore in $TiSe_2$, at least, whether the existence of the CDW should exclude the presence of superconductivity should not a priori be expected, and in fact is clearly not the current case. The interesting electronic picture for electron-doped doped 1T- $TiSe_2$ is further elaborated through our ARPES characterization of the electronic structures of $Ti_{0.85}Nb_{0.15}Se_2$ and $Ti_{0.85}Ta_{0.15}Se_2$, described below.

In **Figures 3a-h** we present the electronic structures of $\text{Ti}_{0.85}\text{Ta}_{0.15}\text{Se}_2$, $\text{Ti}_{0.85}\text{Nb}_{0.15}\text{Se}_2$ and pristine 1T-TiSe_2 determined in the ARPES experiments, which were performed at 15 K. Fermi surface cuts at the border of the Brillouin zone in the plane containing the high-symmetry points A, L, and H, at $k_c \sim \pi/c$, are shown in **Figure 3a** for $\text{Ti}_{0.85}\text{Ta}_{0.15}\text{Se}_2$ and **3b** for $\text{Ti}_{0.85}\text{Nb}_{0.15}\text{Se}_2$. The cuts show the petal-like electron Fermi surfaces from the conduction bands, analogous to what is seen in Cu_xTiSe_2 .³⁹ The direct comparison shows the qualitatively smaller electron Fermi surface for the case of Nb doping, even though the chemically equivalent dopants are expected to be electronically identical as well. Panels **3c** and **3d** show the band dispersions across the electron pocket at L for $\text{Ti}_{0.85}\text{Ta}_{0.15}\text{Se}_2$ and $\text{Ti}_{0.85}\text{Nb}_{0.15}\text{Se}_2$, demonstrating the similarity in the dispersions, but again illustrating the smaller filling of the electron pocket in the Nb-doping case. Estimates of the n-type carrier concentrations from the sizes of the Fermi surfaces are $\sim 1 \times 10^{21} \text{ cm}^{-3}$ for $\text{Ti}_{0.85}\text{Nb}_{0.15}\text{Se}_2$ and $4 \times 10^{21} \text{ cm}^{-3}$ for $\text{Ti}_{0.85}\text{Ta}_{0.15}\text{Se}_2$, ARPES was used to study the character of the top of the valence band, that is, the bands forming the hole pockets in the center of the k_c -projected Brillouin zone for **3e** $\text{Ti}_{0.85}\text{Ta}_{0.15}\text{Se}_2$ and **3f** $\text{Ti}_{0.85}\text{Nb}_{0.15}\text{Se}_2$. These bands exhibit a noticeable reduction of the spectral intensity approximately 100 meV below the Fermi level. Some calculate this to be the signature of a CDW phase with moderate to strong excitonic effects.³⁶

A general comparison between the cases of 1T-TiSe_2 and Nb-doped TiSe_2 is shown in panels **3g** and **3h**. The results for 1T-TiSe_2 **3g** show what is so unusual about the electronic structure of this material – the band folding due to the CDW is reflected in the fact that at the M point in the Brillouin zone the valence band and the conduction band almost “touch” at E_F with an electronic deformation (i.e. deviation from simple parabolic behavior) at the bottom of the conduction band.³³ Thus the low temperature electronic structure of 1T-TiSe_2 is not analogous to what is seen for the “Fermi surface nesting” scenario displayed by other layered TMDCs with CDW transitions, such as NbSe_2 .⁴⁰ Comparison of the 1T-TiSe_2 electronic structure (**3g**) to the case of the Nb doping (**3h**) shows that, as expected, the electrons donated by Nb result in significant occupancy of the conduction band. Just like pristine TiSe_2 , the doped samples show the hole-like band replicated below the electron pocket at M - however, with considerably lower spectral intensity. We note finally that there is a considerably larger energy overlap between the hole-like bands around $\Gamma(\text{A})$ and the

electron pockets around M(L) in Ta- and Nb- doped TiSe₂ than in either pristine 1T-TiSe₂, or 1T-TiSe₂ intercalated with Cu.⁴²

Because superconductivity ultimately arises from electron-phonon coupling in conventional materials, we look further into the potential differences between the doped systems by comparing their phonon spectra, probed by Raman scattering, to that of undoped TiSe₂. The Raman spectra for 1T-TiSe₂ and the 15% Nb and Ta doped samples are shown in **Figure 3i**. The 1T-TiSe₂ Raman spectrum is in good agreement with previously published studies^{43,44}. Specifically, we observe a strong A_{1g} peak at 200 cm⁻¹ and an E_g peak at 136 cm⁻¹ (the symmetries were established in previous studies). The Nb-doped sample produces a near identical spectrum to that of undoped TiSe₂. Interestingly, the E_g mode is unaffected by Ta-doping, while two significant differences are observed near the A_{1g} mode. Specifically, the A_{1g} mode shifts to lower energies, while a new mode appears above it. This is best seen in **Figure 3j** where we focus on just the region near the A_{1g} mode. By fitting with two Lorentzians, we find that the A_{1g} mode has been shifted down to ~197 cm⁻¹ while a new mode has appeared at ~213 cm⁻¹. The shift of the A_{1g} mode to lower energies is consistent with previous studies of 1T-TaSe₂, where the mode is found at 190 cm⁻¹ with no others in this range⁴⁵. 1T-TaSe₂ has only been measured in its commensurate CDW state. Nonetheless, from group theory, we would not expect an additional mode in the absence of a CDW distortion. 2H-TaSe₂ does possess a mode very close to the observed new mode, but 2H-TaSe₂ could not be present as a separate phase because it would display two additional modes in the studied frequency range (at 210 cm⁻¹ and at 240 cm⁻¹)⁴⁶. Given the high doping levels in Ti_{0.8}Ta_{0.2}Se₂ this could instead be a local defect induced mode resulting from the Ta doping. Ta is quite a bit heavier than Ti, however and as such is expected to produce local modes below the bulk modes and not above as is observed here. Ultimately further studies using polarization and/or temperature dependence could potentially rule out the different scenarios for the origin of this mode. Nonetheless, the emergence of superconductivity in Ta doped TiSe₂, and its absence with similar levels of Nb doping may, in addition to the differences in the electronic densities of states, also lie in the difference in the way these dopants modify the phonon modes of the materials.

Finally, the electronic phase diagram as a function of temperature and doping level for many electron-doped 1T-TiSe₂ systems is summarized in **Figure 4**. For comparison to the present results for 1T-Ti_{1-x}Ta_xSe₂ and 1T-Ti_{1-x}Nb_xSe₂ the electronic

phase diagrams for Cu_xTiSe_2 and Pd_xTiSe_2 are included in the figure. The CDW signature in the resistivity gets weaker with higher x content in $\text{Ti}_{1-x}\text{Ta}_x\text{Se}_2$, and the CDW transition is driven down only slightly in temperature. This is different from the case in Cu_xTiSe_2 , in which the CDW transition in TiSe_2 is driven down substantially in temperature with increasing Cu content, followed by the emergence of a superconducting state.¹³ In the $\text{Ti}_{1-x}\text{Ta}_x\text{Se}_2$ system, the x dependence of T_c displays a dome-like shape that is broad in composition. The superconducting state appears for $x > 0.02$, going through a maximum T_c of 2.2 K at $x = 0.2$, followed by a decrease of T_c and then disappearance when at $x > 0.5$. Compared with Cu_xTiSe_2 , the maximum T_c in $\text{Ti}_{1-x}\text{Ta}_x\text{Se}_2$ is lower but the superconducting region is much broader. In addition, there is a significant boundary composition region ($0.02 < x < 0.2$) where superconductivity and CDW behavior may coexist. For the isoelectronic equivalent material $\text{Ti}_{1-x}\text{Nb}_x\text{Se}_2$, on the other hand, superconductivity does not appear for temperatures above 0.4 K for any of the materials. For the Pd-intercalated system, Pd_xTiSe_2 , T_c is low and is found for only a narrow composition range.²⁴

Conclusion

We have found that TiSe_2 becomes superconducting when doped with Ta, a dopant which, consistent with a simple chemical picture, donates electrons to the conduction band. ARPES characterization of the resulting material shows that the Fermi surface is very similar to that seen for Cu-intercalated TiSe_2 . The T_c for the Ta doped case is a factor of 2 lower than that observed for Cu intercalation and is seen over a much wider range of electron doping concentrations. For chemically equivalent and chemically isoelectronic Nb doping, on the other hand, the phonon spectrum and the electronic system do appear to be significantly different. The smaller observed γ is consistent with the observation that the Fermi surface and conduction band filling are significantly smaller in the Nb doped case than it is seen in the Ta doped case. That in itself would not obviously lead to the absence of superconductivity, since it emerges in other doped 1T- TiSe_2 systems at very low electron doping levels (i.e. $x \sim 0.02$), where the filling of the conduction band and thus the size of the electron Fermi surface is very small. The data overall imply that although chemically equivalent, the Nb dopant is not as effective in donating electrons into the conduction band of 1T- TiSe_2 as the Ta dopant is, even though it does weaken the CDW. Our comparison of the electronic phase diagrams for the different types of electron doping of 1T- TiSe_2

finds them to be quite different, clearly showing that how one chemically dopes electrons into the 1T-TiSe₂ system strongly matters. Although differences in the underlying electronic and phonon systems are observed, the fundamental reasons behind why Ta and Nb doping should lead to such differences remain obscure. The big difference between Nb and Ta doping in inducing superconductivity in the present material may have broad implications for doping-induced superconductivity in conventional electronic systems in general because failed attempts to introduce superconductivity in a material through chemical substitution may succeed if a different dopant is employed, or may be specific to the case of 1T-TiSe₂, which has certainly proven to be an unusual electronic material, and would be of interest for further study. We conclude by pointing out that while intercalation-induced superconductors such as 1T Cu_xTiSe₂ or Pd_xTiSe₂ may not be suitable for exfoliation and the fabrication of experimental devices due to the difficulty in cleaving TMDCs with intercalants that strongly bond the layers together, Ta-doped 1T-TiSe₂ is likely to be highly suitable for that purpose since the van der Waals bonding between MX₂ layers remains undisturbed in the superconducting material and exfoliation is expected to be relatively easy.

Acknowledgements

The materials synthesis and physical property characterization of this superconductor were supported by the Department of Energy, division of basic energy sciences, Grant DE-FG02-98ER45706. The single crystal structure determinations were supported by the Gordon and Betty Moore Foundation, EPiQS initiative, grant GBMF4412. The electron diffraction study at Brookhaven National Laboratory was supported by the DOE BES, by the Materials Sciences and Engineering Division under Contract DE-AC02-98CH10886, and through the use of the Center for Functional Nanomaterials. The ARPES experiments were performed under the LBNL and BNL grants DE-AC02-05CH11231 and DE-SC0012704. The Raman spectroscopy, AFM and mechanical exfoliation was supported by the National Science Foundation, Grant DMR-1410846.

Author Contributions

R.J.C and H.X.L conceived and designed the experiments and H.X.L performed the synthetic experiments and H.X.L and R.J.C analyzed and interpreted the chemical and transport data. W.W.X performed and analyzed the single diffraction data. H.X.L, E M.S and J.K performed and analyzed the XRD refinement data. J.T. and Y.M.Z performed and analyzed the electron diffraction data. I.P. and T.V. performed the ARPES measurements and analysis. G.O. and K.B. performed the Raman spectroscopy measurements and analyzed the Raman data. G.S.S. performed the XPS

spectra measurements and analyzed the XPS data. H.X.L and R.J.C wrote the paper with input from all authors. All authors approved the content of the manuscript.

Competing financial interests: The authors declare no competing financial interest.

References

1. Withers, R. L.; Bursil, L. A. The structure of the incommensurate superlattices of 2H-TaSe₂. *Philosophical Magazine*, **1981**, *B43(4)*, 635-672.
2. Arguello, C. J.; Chockalingam, S. P.; Rosenthal, E. P.; Zhao, L.; Gutiérrez, C.; Kang, J. H.; Chung, W. C.; Fernandes, R. M.; Jia, S.; Millis, A. J.; Cava, R. J.; Pasupathy, A. N. Visualizing the charge density wave transition in 2H-NbSe₂ in real space. *Phys. Rev. B* 2014, *89(23)*, 235115-235123.
3. Soumyanarayana, A.; Yee, M. M.; He, Y.; van Wezel, J.; Rahne, D. J.; Rosnagel, K.; Hudson, E. W.; Norman, M. R.; and Hoffman, J. E. Quantum phase transition from triangular to stripe charge order in NbSe₂. *Proc Natl Acad Sci USA*, **2013**, *110(10)*, 1623-1627.
4. Malliakas, C. D.; Kanatzidis, M. G.; Nb-Nb Interactions define the charge density wave structure of 2H-NbSe₂. *J. Am. Chem. Soc.* **2013**, *135(5)*, 1719-1722.
5. Levy, F.; and Froidevaux, Y. Structural and electrical properties of layered transition metal selenides V_xTi_{1-x}Se₂, and Ta_xTi_{1-x}Se₂. *J. Phys. C: Solid State Phys.* **1979**, *12*, 473-487.
6. Ugeda, M. M.; Bradley, A. J.; Shi, S. F.; da Jornada, F. H.; Zhang, Y.; Qiu, D. Y.; Ruan, W.; Mo, S. K.; Hussain, Z.; Shen, Z.X.; Wang, F.; Louie, S. G.; Crommie, M. F. Giant bandgap renormalization and excitonic effects in a monolayer transition metal dichalcogenide semiconductor. *Nat. Mater.* **2014**, *13*, 1091-1095.
7. Wan, C.; Gu, X.; Dang, F.; Itoh, T.; Wang, Y.; Sasaki, H.; Kondo, M.; Koga, K.; Yabuki, K.; Snyder, G. J.; Yang, R.; Koumoto, K. Flexible n-type thermoelectric materials by organic intercalation of layered transition metal dichalcogenide TiS₂. *Nat Mater.* **2015**, *14*, 622-627.
8. Ali, M. N.; Xiong, J.; Flynn, S.; Tao, J.; Gibson, Q. D.; Schoop, L. M.; Liang, T.; Haldolaarachchige, N.; Hirschberger, M.; Ong, N. P.; Cava, R. J. Large, non-saturating magnetoresistance in WTe₂. *Nature*, **2014**, *514*, 205-208.
9. Luo, H. X.; Xie, W. W.; Tao, J.; Inoue, H.; Gyenis, A.; Krizan, J. W.; Yazdani, A.; Zhu, Y. M.; and Cava, R. J. Polytypism, polymorphism, and superconductivity in TaSe_{2-x}Te_x. *Proc Natl Acad Sci USA*, **2015**, *112(11)*, E1174-E1180.

10. Nagata, S.; Aochi, T.; Abe, T.; Ebisu, S.; Hagino, T.; Seki, Y.; Tsutsumi, K. Superconductivity in the layered compound 2H-TaS₂. *J Phys Chem Solids* **1992**, *53*, 1259- 1263.
11. Fang, L.; Zou, P. Y.; Wang, Y.; Tang, L.; Xu, Z.; Chen, Dong H.; Shan, C., L.; Wen, H.H. Competition of superconductivity and charge density wave order in Na_xTaS₂ single crystals. *Sci. Tech. Adv. Mater.* **2005**, *6*, 736-739.
12. Wagner, K. E.; Morosan, E.; Hor, Y. S.; Tao, J.; Zhu, Y.; Sanders, T.; McQueen, T. M.; Zandbergen, H. W.; Williams, A. J.; West, D. V.; Cava, R. J. Tuning the Charge Density Wave and Superconductivity in Cu_xTaS₂. *Phys. Rev. B* **2008**, *78*, 104520.
13. Morosan, E.; Zandbergen, H. W.; Dennis, B. S.; Bos, J. W. G.; Onose, Y.; Klimczuk, T.; Ramirez, A. P.; Ong, N. P.; Cava, R. J. Superconductivity in Cu_xTiSe₂. *Nat. Phys.* **2006**, *2*, 544-550.
14. Kusmartseva, A. F.; Sipos, B.; Berger, H.; Forró, L.; Tutiš, E. Pressure Induced Superconductivity in Pristine 1T-TiSe₂. *Phys. Rev. Lett.* **2009**, *103*, 236401-236404.
15. Joe, Y. I.; Chen, X. M.; Ghaemi, P.; Finkelstein, K. D.; de la Pena, G. A.; Gan, Y.; Lee, J. C. T.; Yuan, S.; Geck, J.; MacDougall, G. J.; Chiang, T. C.; Cooper, S. L.; Fradkin, E.; Abbamonte, P. Emergence of charge density wave domain walls above the superconducting dome in 1T-TiSe₂. *Nat. Phys.* **2014**, *10*, 421-425,
16. Sipos, B.; Kusmartseva, A. F.; Akrap, A.; Berger, H.; Forro, L.; Tutis, E. From Mott state to superconductivity in 1T-TaS₂. *Nat. Mater.* **7**, 2008, 960- 965.
17. Singh, Y.; Nirmala, R.; Ramakrishnan, S.; Malik, S. K. Competition between superconductivity and charge-density-wave ordering in the Lu₅Ir₄(Si_{1-x}Ge_x)₁₀ alloy system. *Phys. Rev. B* **2005**, *72*, 045106-045113.
18. Ye, J. T.; Zhang, Y. J.; Akashi, R.; Bahramy, M. S.; Arita, R. and Iwasa, Y. Superconducting Dome in a Gate-Tuned Band Insulator. *Science*, **2012**, *338* (6111), 1193-1196.
19. Salvo, Di, F. J.; Moncton, D. E.; Waszczak, J. V. Electronic properties and superlattice formation in the semimetal TiSe₂. *Phys. Rev. B* **1976**, *14*, 4321-4328.
20. Stoffel, N. G.; Kevan, S. D.; Smith, N. V. Experimental band structure of 1T-TiSe₂ in the normal and charge-density-wave phases. *Phys. Rev. B* **1985**, *31*, 8049-8055.

21. Myron, H. W.; Freeman, A. J. Electronic structure and optical properties of layered dichalcogenides: TiS_2 , and TiSe_2 , *Phys. Rev. B* **9**, **1974**, 9(2), 481-486.
22. Wilson, J. A. Concerning the semimetallic characters of TiS_2 and TiSe_2 . *Solid State Comm.* **1977**, *22*, 551-553.
23. Kidd, T. E.; Miller, T.; Chou, M. Y.; Chiang, T. C. Electron-Hole Coupling and the Charge Density Wave Transition in TiSe_2 . *Phys. Rev. Lett.* **2002**, *88*, 226402-226406.
24. Morosan, E.; Wagner, K. E.; Zhao, L. L.; Hor, Y.; Williams, A. J.; Tao, J.; Zhu, Y.; Cava, R. J. Multiple electronic transitions and superconductivity in Pd_xTiSe_2 . *Phys. Rev. B* **2010**, *81*, 094524.
25. Ni, N.; Tillman, M.; Yan, J. Q.; Kracher, A.; Hannahs, S.; Bud'ko, S.; Canfield, P. Effects of Co substitution on thermodynamic and transport properties and anisotropic H_{c2} in $\text{Ba}(\text{Fe}_{1-x}\text{Co}_x)_2\text{As}_2$ single crystals. *Phys. Rev. B* **2008**, *78*, 214515.
26. Ni, N.; Thaler, A.; Yan, J.; Kracher, A.; Colombier, E.; Bud'ko, S.; Canfield, P.; Hannahs, S. Temperature versus doping phase diagrams for $\text{Ba}(\text{Fe}_{1-x}\text{TM}_x)_2\text{As}_2$ (TM = Ni, Cu, Co) single crystals. *Phys. Rev. B* **2010**, *82*, 024519.
27. Ni, N.; Thaler, A.; Kracher, A.; Yan, J.; Bud'ko, S.; Canfield, P. Phase diagrams of $\text{Ba}(\text{Fe}_{1-x}\text{M}_x)_2\text{As}_2$ single crystals (M = Rh and Pd), *Phys. Rev. B* **2009**, *80*, 024511.
28. Rodríguez-Carvajal, J. Recent developments of the program FULLPROF. *Comm. Powder Diffr.* **2001**, *26*, 12-19.
29. Suzer, S. Differential Charging in X-ray Photoelectron Spectroscopy: A Nuisance or a Useful Tool? *Anal. Chem.* **2003**, *75*, 7026-7029.
30. Zhao, J. F.; Ou, H. W.; Wu, G.; Xie, B. P.; Zhang, Y.; Shen, D. W.; Wei, J.; Yang, L. X.; Dong, J. K.; Arita, M.; Namatame, H.; Taniguchi, M.; Chen, X. H.; Feng, D. L. Evolution of the Electronic Structure of $1\text{T-Cu}_x\text{TiSe}_2$. *Phys. Rev. Lett.* **2007**, *99*, 146401-146404.
31. Donkov, N.; Mateev, E.; Safonov, V.; Zykova, A.; Yakovin, S.; Kolesnikov, D.; Sudzhanskaya, I.; Goncharov, I.; Georgieva, V. Comparative analysis of electrophysical properties of ceramic tantalum pentoxide coatings, deposited by electron beam evaporation and magnetron sputtering methods. *J. Phys.: Conf. Ser.* **2014**, *558*, 012036.

32. Maria, A. B.; Gomes, L. O. de S. B.; Sandra, C. de C.; Damião, A. J. The Electrochromic Process at Nb₂O₅ Electrodes Prepared by Thermal Oxidation of Niobium. *J. Electrochem. Soc.* **1990**, *137*, 3067-3070.
33. Luo, H.X.; Krizan, J. W.; Seibel, E. M.; Xie, W.; Sahasrabudhe, G. S.; Bergman, S. L.; Phelan, B. F.; Tao, J.; Wang, Z.; Zhang, J.; Cava, R. J. Cr-Doped TiSe₂-A Layered Dichalcogenide Spin Glass. *Chem. Mater.* 2015, **27**, 6810-6817.
34. Mott, N.F. Conduction in non-crystalline materials. *Phil. Mag.* **1969**, *19*, 835-852.
35. Barath, H.; Kim, M.; Karpus, J. F.; Cooper, S. L.; Abbamonte, P.; Fradkin, E.; Morosan, E.; Cava, R. J. Quantum and Classical Mode Softening Near the Charge-Density-Wave-Superconductor Transition of Cu_xTiSe₂. *Phys. Rev. Lett* 2008, **100**, 106402-106406,
36. Wilson, J. A.; Barker, A. S.; Salvo, F. J. D.; Ditzenberger, J. A. Infrared properties of the semimetal TiSe₂. *Phys. Rev. B* **1978**, *18*, 2866-2875.
37. Kohn, W. Excitonic Phases, *Phys. Rev. Lett.* **1967**, *19*, 439-442.
38. Luo, H. X.; Klimczuk, T.; Mühler, L.; Schoop, L.; Hirai, D.; Fuccillo, M. K.; Felser, C.; Cava, R. J. Superconductivity in the Cu(Ir_{1-x}Pt_x)₂Se₄ spinel. *Phys Rev B* **2013**, *87*, 214510.
39. Monney, C.; Schwier, E. F.; Garnier M. G.; Mariotti, N.; Didiot, C.; H Cercellier, H.; Marcus, J.; Berger, H.; Titov, A N.; Beck, H. Probing the exciton condensate phase in 1T-TiSe₂ with photoemission. *New J. Phys.* 2010, **12**, 125019.
40. Rohwer, T.; Hellmann, S.; Wiesenmayer, M.; Sohr, C.; Stange, A.; Slomski, B.; Carr, A.; Liu, Y.; Avila, L. M.; Kallane, M.; Mathias, S.; Kipp, L.; Rossnagel, K.; Bauer, M. Collapse of long-range charge order tracked by time-resolved photoemission at high momenta. *Nature*, **2011**, *471*, 490-493.
41. Kiss, T.; Yokoya, T.; Chainani, A.; Shin, S.; Hanaguri, T.; Nohara, M.; Takagi, H. Charge-order-maximized momentum-dependent superconductivity. *Nat. Phys.* **2007**, *3*, 720-725.
42. Qian, D.; Hsieh, D.; Wray, L.; Morosan, E.; Wang, N.;L.; Xia, Y.; Cava, R.;J. and Hasan, M. Z.; Emergence of Fermi pockets in an excitonic CDW melted novel superconductor. *Phys. Rev. Lett.* **2007**, *98*, 117007.
43. Holy, J. A.; Woo, K. C.; Klein, M. V.; Brown, F. C. Raman and infrared studies of superlattice formation in TiSe₂. *Phys. Rev. B* **1977**, *16*, 3628.

44. Sugai, S.; Murase, K.; Uchida, S.; Tanaka, S. Raman studies of lattice dynamics in 1T-TiSe₂. *Solid State Comm.* **1980**, *35*, 433-436.
45. Layne, C. B.; Lowdermilk, W. H.; Weber, M. J. Multiphonon relaxation of rare-earth ions in oxide glasses. *Phys. Rev. B*, **1977**, *16*, 10.
46. Smith, Jr, J. E.; Tsang, J. C.; Shafer, M. W. Raman spectra of several layer compounds with charge density waves. *Solid State Comm.* **1976**, *19*, 283-286.

Figures legends

Figure 1 Structural and chemical characterization of $\text{Ti}_{1-x}\text{Ta}_x\text{Se}_2$, $\text{Ti}_{1-x}\text{Nb}_x\text{Se}_2$ (a) Powder XRD patterns (Cu $K\alpha$) for selected samples (TiSe_2 , $\text{Ti}_{0.8}\text{Ta}_{0.2}\text{Se}_2$ and $\text{Ti}_{0.8}\text{Nb}_{0.2}\text{Se}_2$) in this study. (b) Composition dependence of the room temperature lattice parameters for $\text{Ti}_{1-x}\text{Ta}_x\text{Se}_2$ ($0 \leq x \leq 0.9$) and $\text{Ti}_{1-x}\text{Nb}_x\text{Se}_2$ ($0 \leq x \leq 0.7$), compared with that of Cu_xTiSe_2 ($0 \leq x \leq 0.11$). Lattice parameters for Cu_xTiSe_2 were extracted from Ref 13. (e,f) XPS spectra of the Nb $3d$ and Ta $4f$ regions of $\text{Ti}_{0.8}\text{Nb}_{0.2}\text{Se}_2$ and $\text{Ti}_{0.8}\text{Ta}_{0.2}\text{Se}_2$. For comparison, the Nb $3d$ and Ta $4f$ spectra for undoped 2H-NbSe₂ and 2H-TaSe₂ are included in (c,d). The shifts in binding energy Δ compared to the absolute binding energy (i.e. $\Delta/\text{B.E.}$) are very similar for both Nb and Ta dopants, showing them to be chemically equivalent when substituted in 1T-TiSe₂. Electron diffraction in the [001] zones (g) and (i) $\text{Ti}_{0.8}\text{Nb}_{0.2}\text{Se}_2$ at room temperature (RT) 300 K and 89 K respectively. (h) and (j) the same two temperatures for $\text{Ti}_{0.8}\text{Ta}_{0.2}\text{Se}_2$. The CDW is present, visible due to its weak diffraction spots, in the Ta doped material at 89 K, but not in the Nb-doped material.

Figure 2 Transport and specific heat characterization of the normal states and superconductivity. (a) The temperature dependence of the resistivity ratio ($\rho/\rho_{300\text{K}}$) for polycrystalline $\text{Ti}_{1-x}\text{Ta}_x\text{Se}_2$ ($0.02 \leq x \leq 0.3$). Inset: $d\rho/dT$ for $\text{Ti}_{1-x}\text{Ta}_x\text{Se}_2$ ($0.05 \leq x \leq 0.25$) in the low temperature region (1 - 3 K), showing the superconducting transition. (b) The temperature dependence of the resistivity ratio ($\rho/\rho_{300\text{K}}$) for polycrystalline $\text{Ti}_{1-x}\text{Nb}_x\text{Se}_2$ ($0.02 \leq x \leq 0.7$) Inset: enlarged view of the low temperature region (0.4 - 3 K), showing the lack of a superconducting transition. (c) Temperature dependence of the resistivity of $\text{Ti}_{1-x}\text{Nb}_x\text{Se}_2$ as $\log \rho$ vs. $\log T$. Red line is a fit to the 2D variable range hopping model at high temperatures. (d) Magnetic susceptibilities of $\text{Ti}_{0.8}\text{Ta}_{0.2}\text{Se}_2$ and $\text{Ti}_{0.8}\text{Nb}_{0.2}\text{Se}_2$ with applied field 5T. Inset: Hall measurement for $\text{Ti}_{0.8}\text{Ta}_{0.2}\text{Se}_2$ and $\text{Ti}_{0.8}\text{Nb}_{0.2}\text{Se}_2$. (e) Temperature dependence of the specific heat C_p of $\text{Ti}_{0.8}\text{Ta}_{0.2}\text{Se}_2$ measured under magnetic fields of 0 T and 5 T, presented in the form of C_p/T vs T^2 (main panel) and C_{el}/T vs T (inset). The green line shows the equal area construction to determine $\Delta C/\gamma T_c$. The red line shows the fit of the specific heat in the range 2 - 10 K at 5 T. (f) Temperature dependence of the specific heat C_p of $\text{Ti}_{0.8}\text{Nb}_{0.2}\text{Se}_2$ measured under a magnetic field of 0 T, presented in the form of C_p/T vs T^2 .

Figure 3. Probing the electronic structure and phonon spectra of the doped 1T-TiSe₂ materials. Performed on the (001) crystal surface ARPES measurements at 15 K and Raman spectra at 300 K. ARPES-determined Fermi surface cuts at the border of the Brillouin zone in the plane containing the high-symmetry points A, L, and H at $k_c \sim \pi/c$ for (a) $\text{Ti}_{0.85}\text{Ta}_{0.15}\text{Se}_2$ and (b) $\text{Ti}_{0.85}\text{Nb}_{0.15}\text{Se}_2$, showing the qualitatively smaller Fermi surface for the case of Nb doping. (c) and (d) The ARPES-determined band dispersion across the electron pocket at L for (c) $\text{Ti}_{0.85}\text{Ta}_{0.15}\text{Se}_2$ and (d) $\text{Ti}_{0.85}\text{Nb}_{0.15}\text{Se}_2$ respectively, again showing the smaller filling of the electron pocket in the Nb-doping case. (e) and (f): The bands forming the hole pockets in the center of the k_c -projected Brillouin zone for (e) $\text{Ti}_{0.85}\text{Ta}_{0.15}\text{Se}_2$ and (f) $\text{Ti}_{0.85}\text{Nb}_{0.15}\text{Se}_2$ respectively. (g) and (h): The band dispersions along Γ -M at $k_c \sim 0$ for pristine 1T-TiSe₂ and Nb-doped TiSe₂, respectively. Spectra were taken at 15 K using photon excitation of 78 eV (a)-(f) and 95 eV (g)-(h). (i) Raman spectra reveal no modification of the phonons of 1T-TiSe₂ by Nb doping and that Ta doping shifts the higher energy A_{1g} mode to lower energies

and induces a new mode at 213 cm^{-1} . (j) Fit of the Raman spectrum in A_{1g} region of $\text{Ti}_{0.85}\text{Ta}_{0.15}\text{Se}_2$ clearly showing the existence of the new mode and the blue shift of the original A_{1g} phonon.

Figure 4 The electronic phase diagram of the superconducting 1T-TiSe₂ system. The electronic phase diagrams for Cu_xTiSe_2 , Pd_xTiSe_2 , $\text{Ti}_{1-x}\text{Ta}_x\text{Se}_2$ and $\text{Ti}_{1-x}\text{Nb}_x\text{Se}_2$ are shown as a function of Cu, Pd, Ta or Nb content x . All the nominally electron-doped systems are different. Superconductor parameters for Cu_xTiSe_2 and Pd_xTiSe_2 were extracted from Refs. 13 and 24, respectively.

Table S1. Single crystal crystallographic data for $\text{Ti}_{0.81}\text{Nb}_{0.19(1)}\text{Se}_2$ and $\text{Ti}_{0.88}\text{Ta}_{0.12(1)}\text{Se}_2$ at 100(2) K.

Table S2. Atomic coordinates and equivalent isotropic displacement parameters of $\text{Ti}_{0.81}\text{Nb}_{0.19}\text{Se}_2$ and $\text{Ti}_{0.88}\text{Ta}_{0.12}\text{Se}_2$ at 100 K. U_{eq} is defined as one-third of the trace of the orthogonalized U_{ij} tensor (\AA^2).

Figure 1S. XPS spectra of the Se $3d$ regions of $\text{Ti}_{0.8}\text{Nb}_{0.2}\text{Se}_2$ and $\text{Ti}_{0.8}\text{Ta}_{0.2}\text{Se}_2$. For comparison, the Se $3d$ spectrum for undoped 2H-NbSe₂ and 2H-TaSe₂ are included in (g,h)

Figure 2S. XPS spectra of the Ti $2p$ regions of $\text{Ti}_{0.8}\text{Nb}_{0.2}\text{Se}_2$ and $\text{Ti}_{0.8}\text{Ta}_{0.2}\text{Se}_2$.

Figure 3S. The upper critical field characterization of $\text{Ti}_{1-x}\text{Ta}_x\text{Se}_2$. Low temperature resistivity at various applied fields for (a) $\text{Ti}_{0.8}\text{Ta}_{0.2}\text{Se}_2$ and (b) $\text{Ti}_{0.85}\text{Ta}_{0.15}\text{Se}_2$. Inset shows the temperature dependence of the upper critical field (H_{c2}).

Figure 1

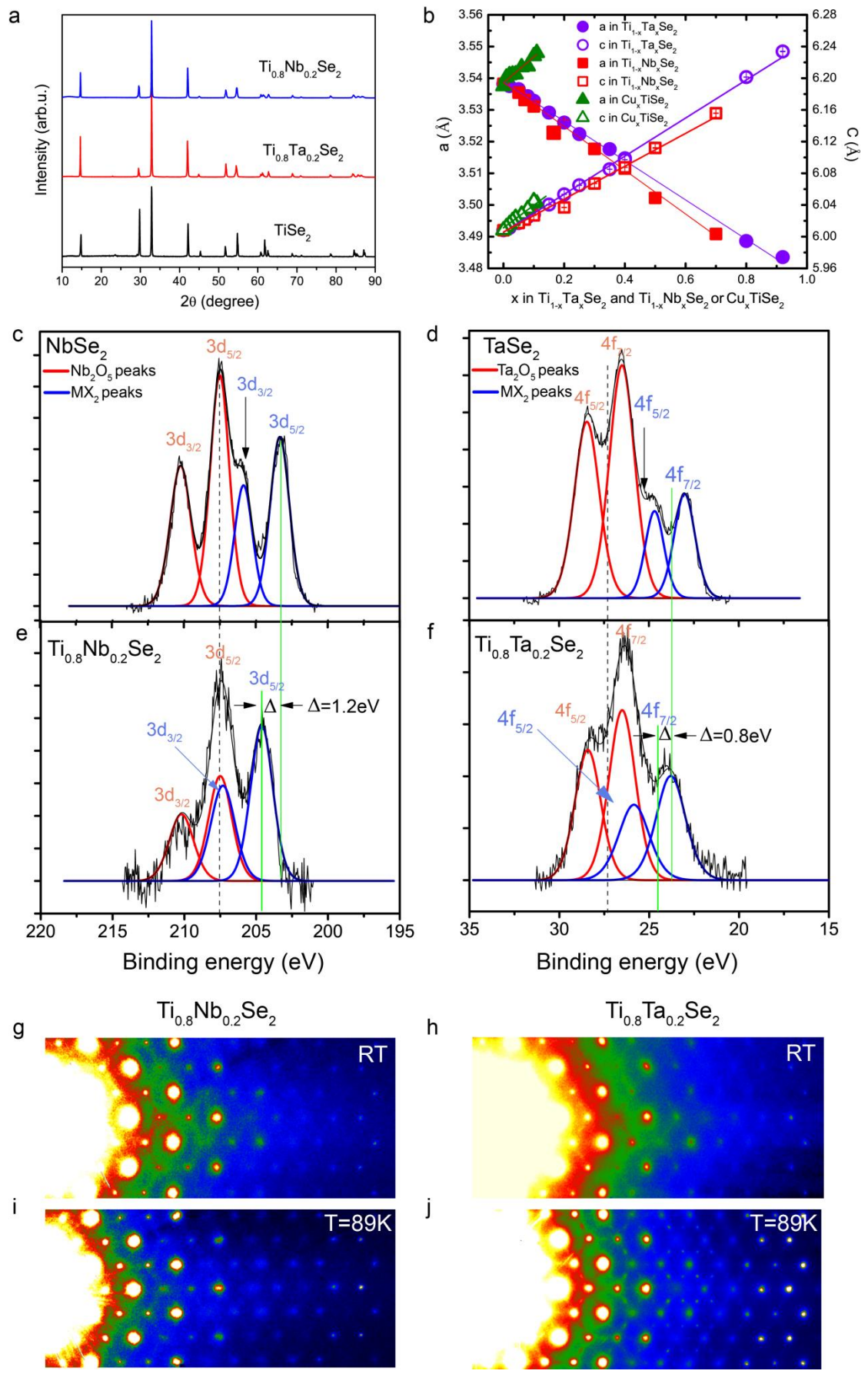


Figure 2

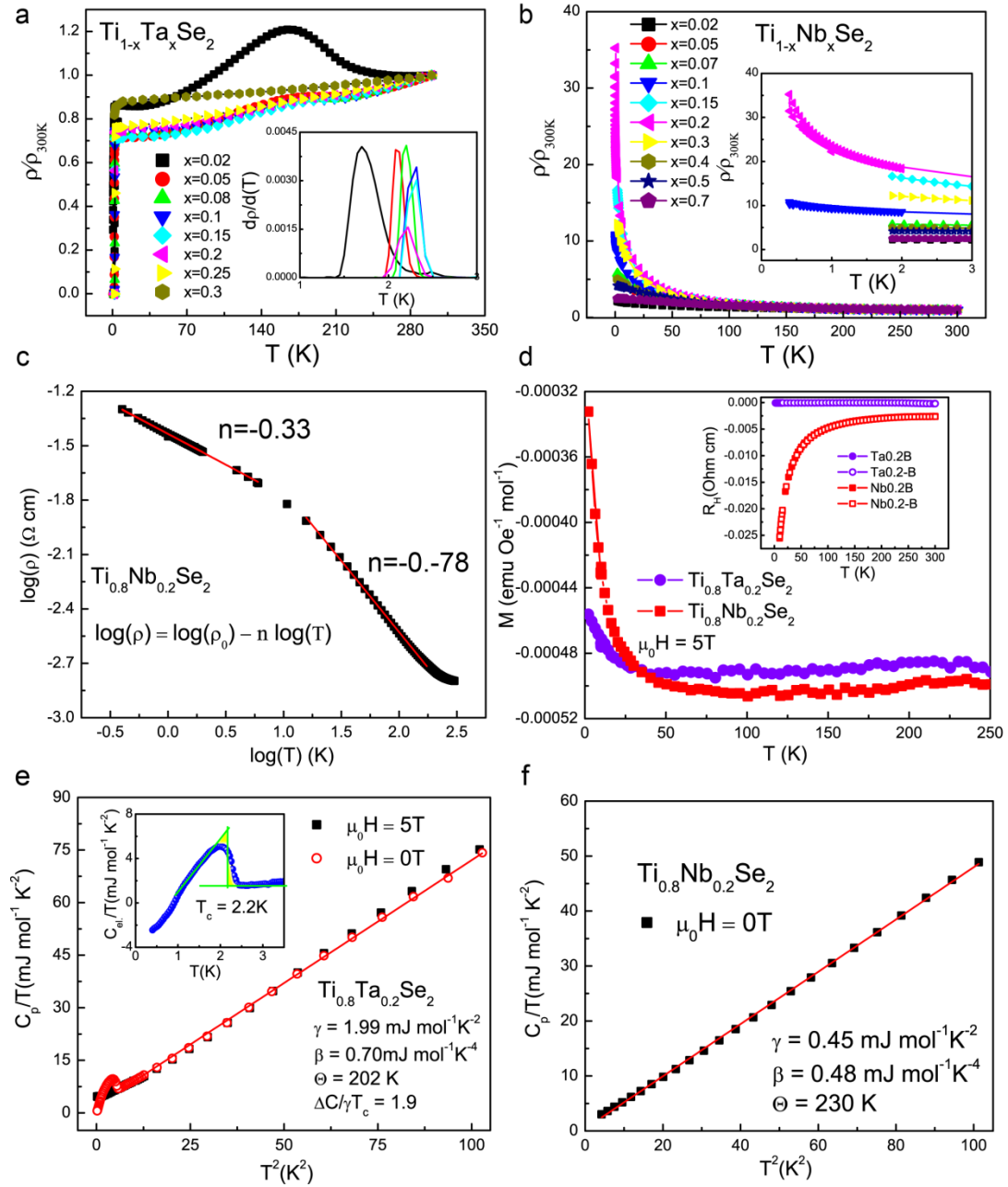


Figure 3

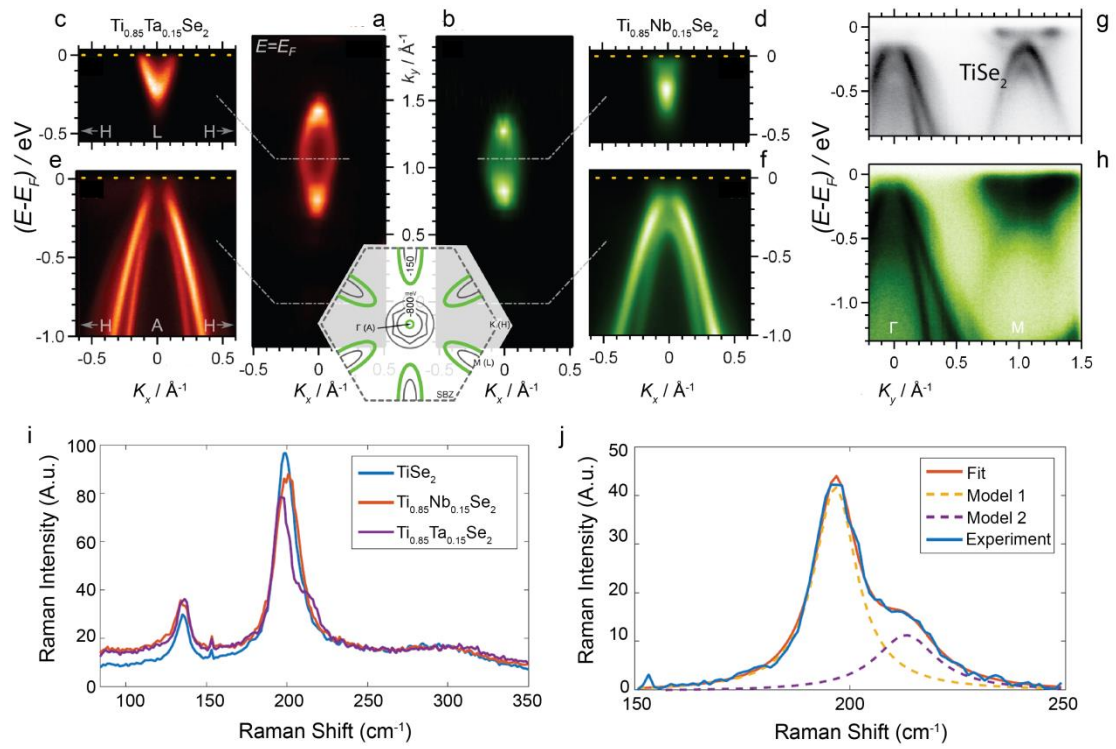


Figure 4

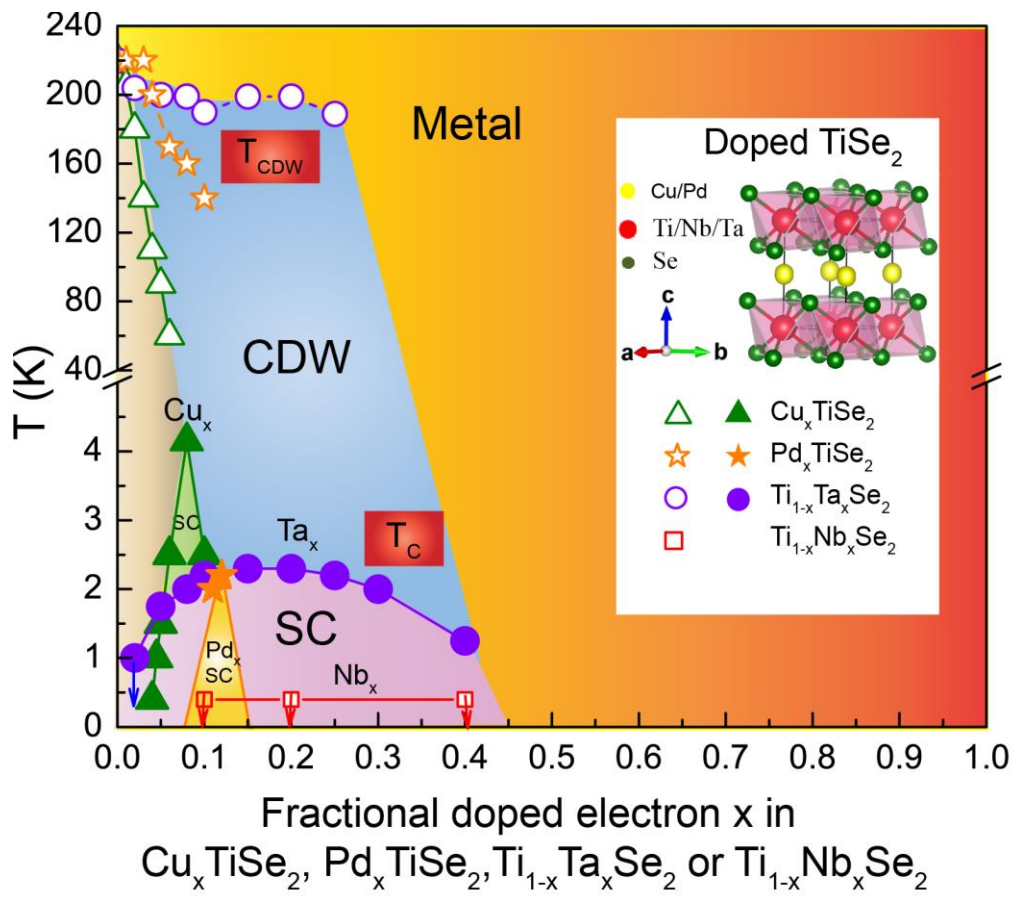
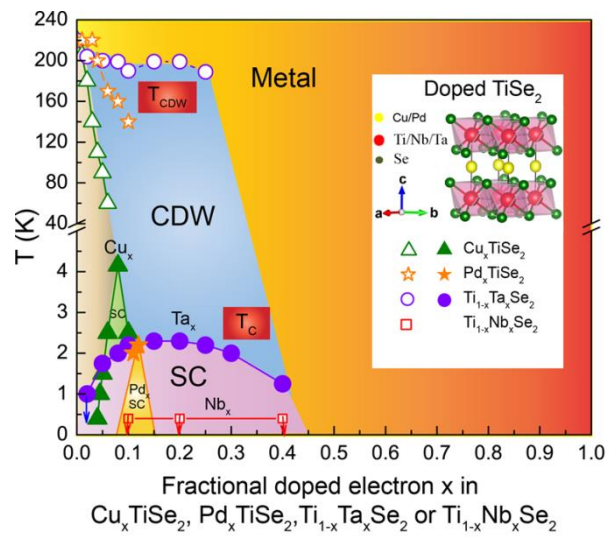


Table of Content

Differences in chemical doping matter - Superconductivity in $\text{Ti}_{1-x}\text{Ta}_x\text{Se}_2$ but not in $\text{Ti}_{1-x}\text{Nb}_x\text{Se}_2$



Supplementary information

Differences in chemical doping matter - Superconductivity in $\text{Ti}_{1-x}\text{Ta}_x\text{Se}_2$ but not in $\text{Ti}_{1-x}\text{Nb}_x\text{Se}_2$

Huixia Luo^{1,*}, Weiwei Xie¹, Jing Tao², Ivo Pletikoscic^{2,3}, Tonica Valla², Girija S. Sahasrabudhe¹, G. Osterhoudt⁴, Erin Sutton⁴, K. Burch⁴, Elizabeth M. Seibel¹, Jason W. Krizan¹, Yimei Zhu² and R. J. Cava¹

¹*Department of Chemistry, Princeton University, Princeton, NJ 08544, USA*

²*Condensed Matter Physics and Materials Science Department, Brookhaven National Lab, Upton, New York 11973, USA*

³*Department of Physics, Princeton University, Princeton, NJ 08544, USA*

⁴*Department of Physics, Boston College, Boston MA*

*huixial@princeton.edu

Crystal Structure analyses

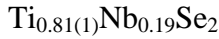
X-ray diffraction intensity data were collected at 100 K on a Bruker Apex Photon diffractometer with Mo radiation $\text{K}\alpha_1$ ($\lambda = 0.71073 \text{ \AA}$) or Cu radiation $\text{K}\alpha_1$ ($\lambda = 1.54098 \text{ \AA}$). Data were collected over a full sphere of reciprocal space with 0.5° scans in ω with an exposure time of 10s per frame. The 2θ range extended from 4° to 60° . The SMART software was used for data acquisition. Intensities were extracted and corrected for Lorentz and polarization effects with the SAINT program. Empirical absorption corrections were accomplished with SADABS, based on modeling a transmission surface by spherical harmonics employing equivalent reflections with $I > 2\sigma(I)$.^{S1-4} Within the SHELXTL package, the crystal structures were solved using direct methods and refined by full-matrix least-squares on F^2 .^{S3}

References

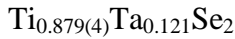
- S1. Sheldrick, G. M. (2001) .SADABS, University of Gottingen, Gottingen,Germany.
- S2. Sheldrick, G. M. (2008) A short history of SHELX. Acta Crystallogr. A 64:112.
- S3. SHELXTL, version 6.10, Bruker AXS Inc.: Madison, WI, 2000.
- S4. Momma K, Izumi F (2011) VESTA 3 for three-dimensional visualization of crystal, volumetric and morphology data. J. Appl. Crystallogr. 44:1272.

Table S1. Single crystal crystallographic data for Nb and Ta doped TiSe₂ at 100(2) K.

Refined Formula	Ti _{0.81(1)} Nb _{0.19} Se ₂	Ti _{0.879(4)} Ta _{0.121} Se ₂
F.W. (g/mol);	214.37	221.79
Space group; <i>Z</i>	<i>P3-m1</i> (No.164); 1	<i>P3-m1</i> (No.164); 1
<i>a</i> (Å)	3.5217(1)	3.5180(2)
<i>c</i> (Å)	6.0443(3)	6.0093(4)
<i>V</i> (Å ³)	64.920(5)	64.409(8)
Absorption Correction	Numerical	Numerical
Radiation	Cu	Mo
Extinction Coefficient	None	None
θ range (deg)	7.327-61.839	3.390-30.045
No. reflections; <i>R</i> _{int}	617;0.0280	810;0.0138
No. independent reflections	53	96
No. parameters	8	8
<i>R</i> ₁ ; <i>wR</i> ₂ (all <i>I</i>)	0.0341; 0.0438	0.0175; 0.0404
Goodness of fit	1.294	1.392
Diffraction peak and hole (e ⁻ /Å ³)	0.636; -1.109	0.953; -1.052

Table S2. Atomic coordinates and equivalent isotropic displacement parameters of Nb and Ta doped TiSe₂ at 100(2) K. *U*_{eq} is defined as one-third of the trace of the orthogonalized *U*_{ij} tensor (Å²).

Atom	Wyckoff.	Occupancy.	<i>x</i>	<i>y</i>	<i>z</i>	<i>U</i> _{eq}
Ta/Ti1	1 <i>a</i>	0.81(1)/0.19	0	0	0	0.0124(13)
Se2	2 <i>d</i>	1	1/3	2/3	0.2581(2)	0.0104(7)



Atom	Wyckoff.	Occupancy.	<i>x</i>	<i>y</i>	<i>z</i>	<i>U</i> _{eq}
Ta/Ti1	1 <i>a</i>	0.879(4)/0.121	0	0	0	0.0059(5)
Se2	2 <i>d</i>	1	1/3	2/3	0.2577(1)	0.0043(2)

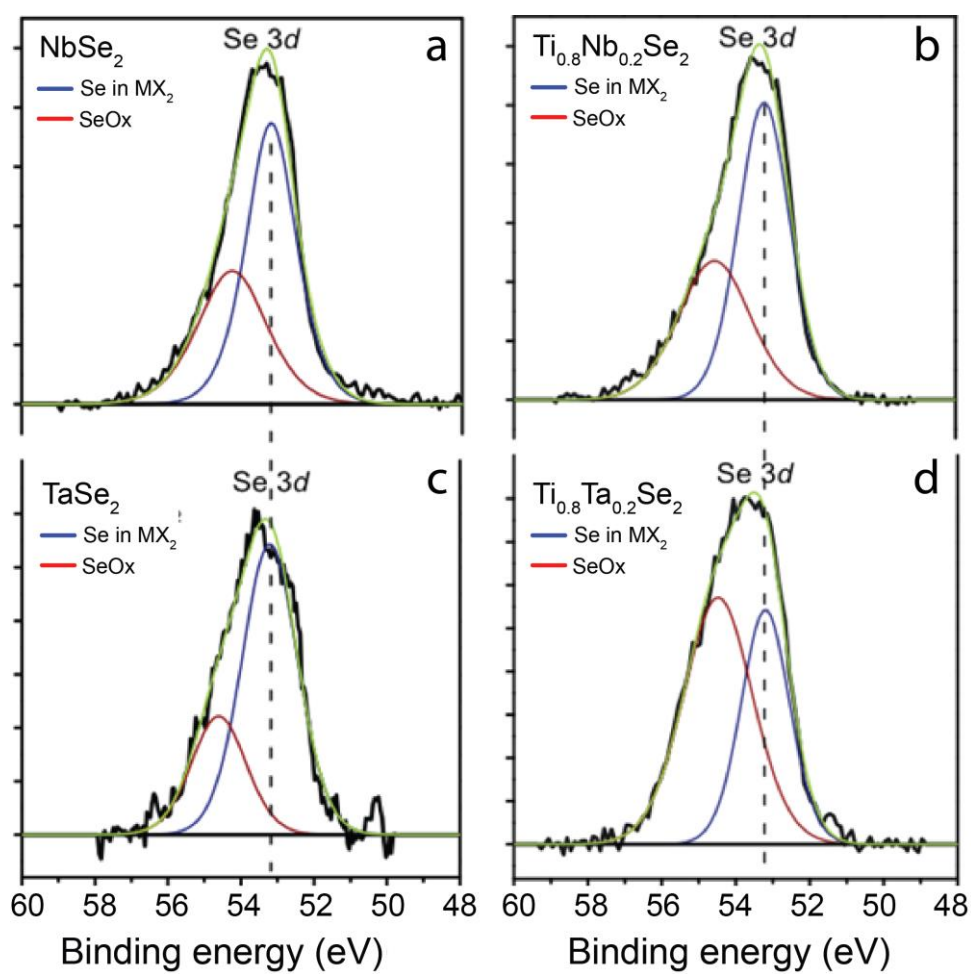


Figure 1S. XPS spectra of the Se 3d regions of Ti_{0.8}Nb_{0.2}Se₂ and Ti_{0.8}Ta_{0.2}Se₂ (c,d). For comparison, the Se 3d spectra for undoped 2H-NbSe₂ and 2H-TaSe₂ are included in (a,b)

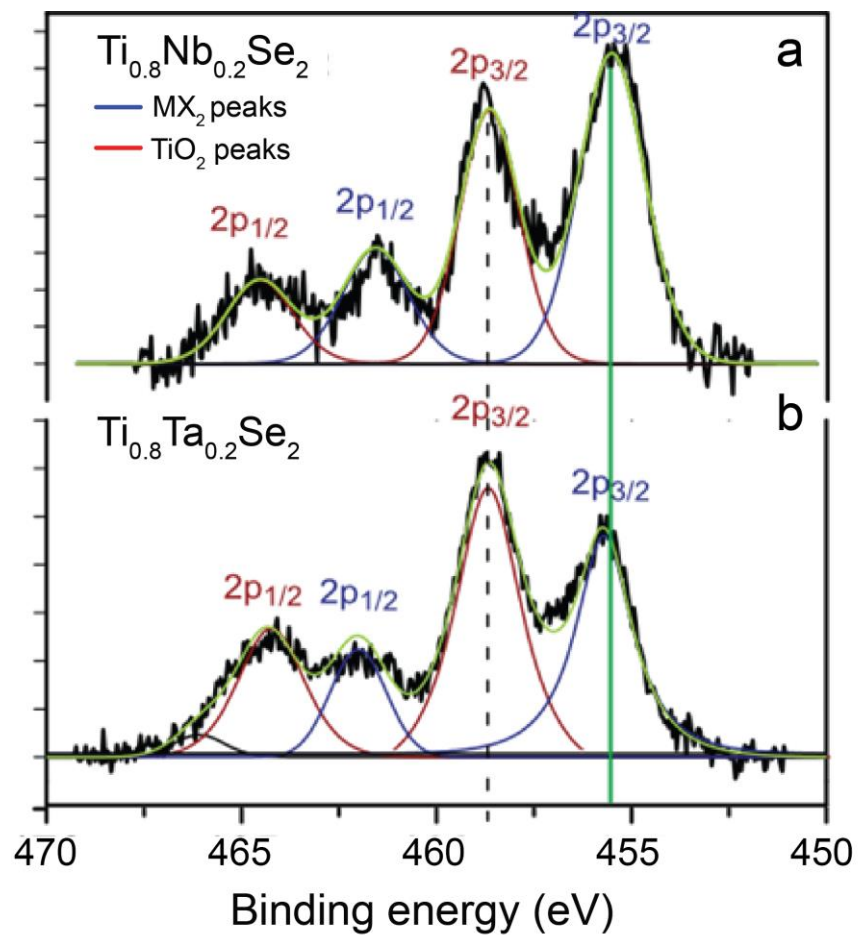


Figure 2S. XPS spectra of the Ti 2p regions of $\text{Ti}_{0.8}\text{Nb}_{0.2}\text{Se}_2$ and $\text{Ti}_{0.8}\text{Ta}_{0.2}\text{Se}_2$.

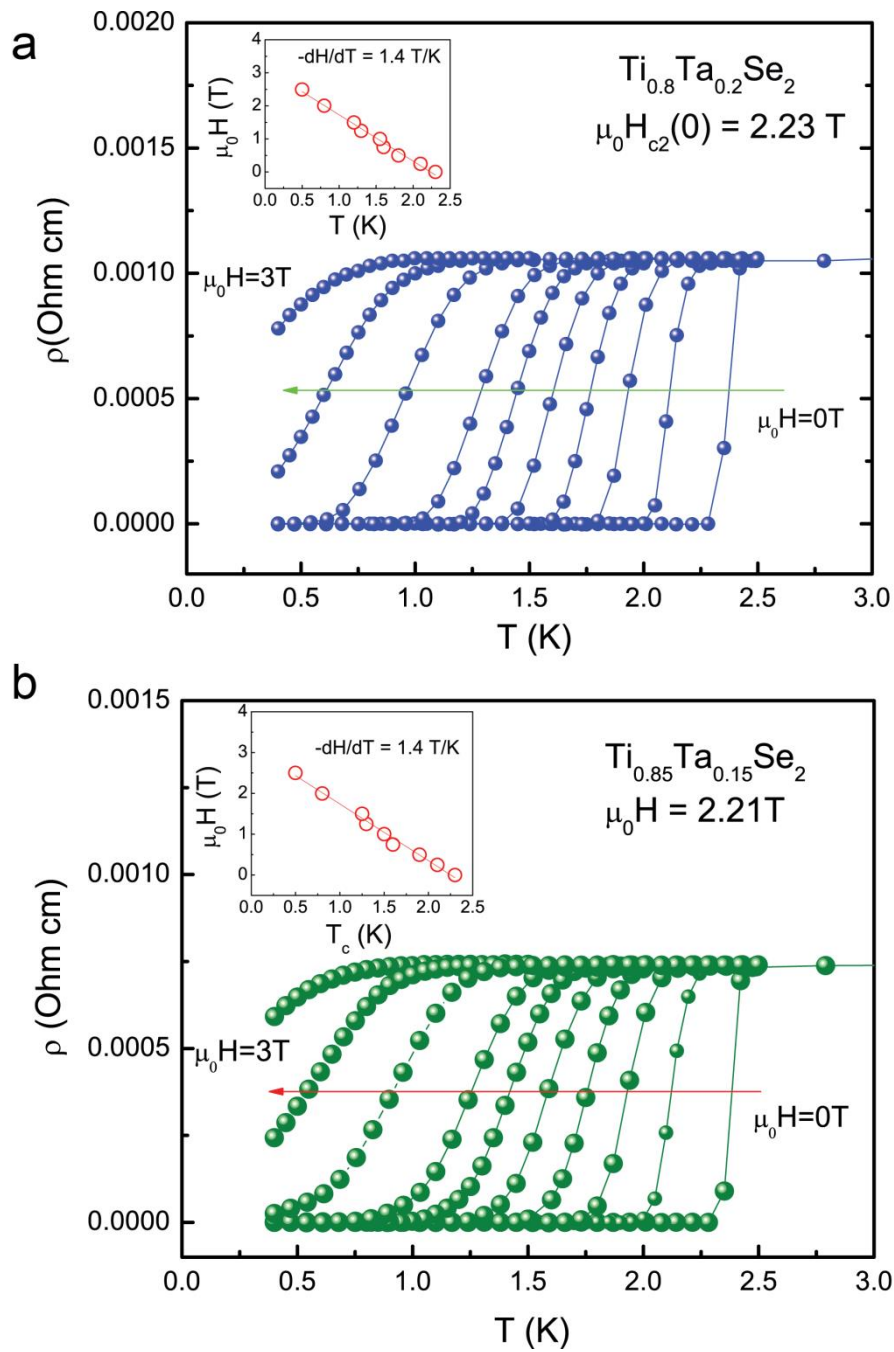


Figure 3S. The upper critical field characterization of $\text{Ti}_{1-x}\text{Ta}_x\text{Se}_2$. Low temperature resistivity at various applied fields for (a) $\text{Ti}_{0.8}\text{Ta}_{0.2}\text{Se}_2$ and (b) $\text{Ti}_{0.85}\text{Ta}_{0.15}\text{Se}_2$. Inset shows the temperature dependence of the upper critical field (H_{c2}).